Retinal Cell Biology

Autophagy and Exocytosis of Lipofuscin Into the Basolateral Extracellular Space of Human Retinal Pigment Epithelium From Fetal Development to Adolescence

Saeed Shahhossein-Dastjerdi,[1,2] Mark E. Koina,[3] George Fatseas,[1] Frank Arfuso,[4] and Tailoi Chan-Ling[1]

[1]Bosch Institute, The University of Sydney, Sydney, Australia
[2]Now at Cell, Tissue & Organ Bank, Forensic Medicine Research Centre, Tehran, Iran
[3]Department of Anatomical Pathology, ACT Pathology, The Canberra Hospital, Canberra, Australia
[4]School of Human Sciences, The University of Western Australia, Crawley, Australia

Correspondence: Tailoi Chan-Ling, Bosch Institute, The University of Sydney, Fisher Rd, Sydney 2006, Australia; tailoi.chan-ling@outlook.com.

Received: March 6, 2023
Accepted: March 6, 2024
Published: April 22, 2024

Citation: Shahhossein-Dastjerdi S, Koina ME, Fatseas G, Arfuso F, Chan-Ling T. Autophagy and exocytosis of lipofuscin into the basolateral extracellular space of human retinal pigment epithelium from fetal development to adolescence. *Invest Ophthalmol Vis Sci.* 2024;65(4):32. https://doi.org/10.1167/iovs.65.4.32

Purpose. To undertake the first ultrastructural characterization of human retinal pigment epithelial (RPE) differentiation from fetal development to adolescence.

Methods. Ten fetal eyes and three eyes aged six, nine, and 17 years were examined in the temporal retina adjacent to the optic nerve head by transmission electron microscopy. The area, number, and distribution of RPE organelles were quantified and interpreted within the context of adjacent photoreceptors, Bruch's membrane, and choriocapillaris maturation.

Results. Between eight to 12 weeks' gestation (WG), pseudostratified columnar epithelia with apical tight junctions differentiate to a simple cuboidal epithelium with random distribution of melanosomes and mitochondria. Between 12 to 26 WG, cells enlarge and show long apical microvilli and apicolateral junctional complexes. Coinciding with eye opening at 26 WG, melanosomes migrate apically whereas mitochondria distribute to perinuclear regions, with the first appearance of phagosomes, complex granules, and basolateral extracellular space (BES) formation. Significantly, autophagy and heterophagy, as evidenced by organelle recycling, and the gold standard of ultrastructural evidence for autophagy of double-membrane autophagosomes and mitophagosomes were evident from 32 WG, followed by basal infoldings of RPE cell membrane at 36 WG. Lipofuscin formation and deposition into the BES evident at six years increased at 17 years.

Conclusions. We provide compelling ultrastructural evidence that heterophagy and autophagy begins in the third trimester of human fetal development and that deposition of cellular byproducts into the extracellular space of RPE takes place via exocytosis. Transplanted RPE cells must also demonstrate the capacity to subserve autophagic and heterophagic functions for effective disease mitigation.

Keywords: age-related macular degeneration, Bruch's membrane, photoreceptors, transmission electron microscopy

Estimates suggest more than 200 million individuals worldwide suffer from vision loss because of retinal pigment epithelium (RPE)-related diseases,[1] reflecting the multiple functional roles subserved by the RPE in the maintenance of vision. Light transduction by photoreceptors is dependent on the proper function and structure of proteins, retinal structures, and membranes. Photoreceptors contain high amounts of photosensitive molecules that are prone to oxidative and photo damage.[2] Thus a constant renewal process is required to maintain the excitability of photoreceptors.[3–5]

This constant renewal of photoreceptor outer segment (POS) is dependent on phagocytosis of shed photoreceptor membranes by the RPE. Every RPE cell is estimated to be in close apposition with 23 photoreceptors at the human fovea, averaged over nine decades.[6] Heterophagy is the specific process of cells recycling material endocytosed from outside the RPE cell.[7,8] In the RPE, shed POS are digested via heterophagic processes,[9] and important molecules, such as retinal or docosahexaenoic acid, are redelivered to photoreceptors, which is supportive of a possible autophagic process to support this molecular recycling.

The superficial zone of the optic cup develops into the RPE by eight weeks' gestation (WG).[10] Immediately upon being functional, the RPE subserve multiple key roles, including formation of the outer blood retinal barrier,

management of fluid transport, regulation of cytokine and growth factor release, processing of reactive oxygen species, recycling of phototransduction components, and regulation of the subretinal space ionic balance.[11–14]

RPE are the most metabolically active cells in the human body because of the continual demands of POS recycling, combined with other digestive processes and active nutrient/waste transport.[15] Autophagy is the process of recycling organelles and damaged proteins within the cell.[8,16] The useful metabolites produced by these processes are translocated to the cytosol, whereas indigestible lysosomal residue contributes to formation of lipofuscin granules, which are eventually exocytosed.[17]

We provide a detailed characterization of human RPE differentiation and the first semiquantitative ultrastructural evidence of autophagy and heterophagy in human fetal RPE in the context of photoreceptor, Bruch's membrane (BrM), and choriocapillaris (ChC) development. Our study showed for the first time that a region exists between RPE cells, present during development, which is the basolateral extracellular space (BES) where cellular digestive byproducts are deposited. The importance of our findings is emphasized by a study showing that dysregulation of autophagy results in abnormal primary cilia, being the underlying pathogenetic mechanism for Leber's congenital amaurosis, an inherited retinal ciliopathy disease that often results in severe visual impairment or blindness in early childhood.[18]

Taken together, the above demonstrates the high unmet need for a treatment for this large population of visually impaired throughout the world as a result of RPE malfunction. It is for this reason that significant resources have been directed toward RPE cell replacement therapies via the transplantation of induced human RPE cells from multipotent human stem cells.[19–21] Our study has significant implications for the field of transplantation of allogenic or autologous induced human RPE cells (ihRPE), where several clinical trials have been investigating the feasibility of transplantation of these cells to mitigate eye diseases involving the RPE[22–24] and may explain the low success of these cell replacement therapies in restoring significant functional improvement of vision. The findings of this study lead us to conclude that transplanted RPE cells must also demonstrate the capacity to subserve autophagic and heterophagic functions for effective disease mitigation.

Material and Methods

A total of 13 eyes aged from eight to 36 WG, and six, nine, and 17 years were analyzed in this study. The morphological observations were made by the two authors (SSD and MEK) independently, and the findings were compared and confirmed by both. All quantitative analyses were undertaken by SSD.

Ten fetal specimens aged eight to 36 WG were prepared by MEK and TCL, as previously reported.[25–30] Three additional specimens aged six, nine, and 17 years were received as donations for research purposes from the Lions Sydney Eye Bank, New South Wales Tissue Banks, New South Wales Organ and Donation Service at the Sydney Eye Hospital for research, after cornea removal for transplantation. These three specimens were de-identified with cause of death being congenital heart disease (six and nine years) and car accident (17 years), with no history of ophthalmic disease. Collection of specimens was covered by the Human Ethics Committee from the University of Sydney protocols: 2006/9063, 2012/15189, 2014/15190 and coordinated with the Lions Sydney Eye Bank, New South Wales Tissue Banks, New South Wales Organ and Donation Service at the Sydney Eye Hospital. The research plan adhered to the tenets of the guidelines set forth in the Declaration of Helsinki.

Morphology, size, and number of specific subcellular organelles; melanosomes in different stages of maturation, mitochondria, phagosomes, complex granules, lipofuscin granules, nuclei, mitophagosome, autophagosome, and autolysosomes were quantified by iTEM software (Olympus Soft Imaging Solutions GmbH, Germany). The TEM and software are calibrated biannually to meet ISO 15189 and ISO 29301 as part of their NATA accreditation, thus ensuring the accuracy of the analysis. Specifically, pixel size at magnification ranges from ×500 to ×100,000 is set during the initial installation of the digital camera system. These remain constant throughout the life of the CCD in the camera. The TEM itself is calibrated twice per year and is within 0.5% of the manufacturer's specifications for the instrument. Calibrations are performed at all changes of filaments and when alignments are performed. Calibration is undertaken using a metrologically traceable standard (MAG*I*CAL).

Because the horizontal diameter of the eye cup increases from approximately 10 mm at 24 WG to 17 mm at 36 WG, similar to the optic nerve head (ONH) broadening, and increasing cell density and dimensions of the antecedent macular region,[31] our region of analyses and collection of samples were undertaken from the area adjacent to the ONH.

After enucleation of the eyes, the anterior segment and vitreous were removed, and the eyecups were immersed fixed in 2% glutaraldehyde in 0.1 M cacodylate buffer (pH 7.4), with extra injections of the fixative into the vitreous at 4°C for 24 hours (primary fixation). The eyes were postfixed in 2% osmium tetroxide in 0.1 M cacodylate buffer (pH 7.4) at room temperature for four hours. Several of the fetal specimens were fixed and stored in 4% paraformaldehyde in 0.1M phosphate buffer pH 7.6, before additional fixation in 2% glutaraldehyde and osmium tetroxide as above. Consequently, image quality was marginally compromised due to extraction of the cytoplasmic content and cristae of the mitochondria. The eyecup was then subjected to a circular and four radial incisions. A circular sampling of 1 mm full thickness was taken from the ONH at 9 o'clock with a disposable 1 mm biopsy punch (BP-10F, Kai Medical, Japan). A second sampling was taken from 9 mm further in the temporal side of 26 to 28 WG specimens to compare regional differentiation of RPE in the ONH and mid-peripheral retina. The sclera was peeled off, and preparation of the specimens for transmission electron microscopy was performed as previously reported.[30] In addition, to evaluate the ChC maturation, five independent locations were assessed per capillary, and 25 capillaries (each ~100 μm^2) observed in total, at six years in both the ONH and mid periphery. A minimum of 50 fields of views (which equates to five images per cell for a total of 10 cells per age) were captured and analyzed. Furthermore, to permit capture of optimal images in support of key findings, an additional 40 fields of views (which equates to five images per cell for a total of eight cells per age) were captured at eight, 10, 24, 26, and 36 WG and six years, corresponding to the youngest specimens studied, onset of eye opening, first evidence of autophagy observed, oldest fetal specimen studied, and the age at which lipofuscin was first observed, respectively. RPE cells at each age were evaluated at low magnification, and their organelles were measured in

high magnified views. Additional post-capture optimization of the contrast and gray range of the images were undertaken using Adobe Photoshop Lightroom Classic - 13.0.2 release, build [202311290958-8ff975ea] software. Finally, the mean ± S.E.M. of all measurements for each different age was analyzed by one-way ANOVA with post-hoc tests, and $P < 0.05$ was considered statistically significant.

Results

Initial RPE Development in First Trimester Between Eight to 12 WG

At eight WG, organelles are randomly distributed in the cytoplasm (Figs. 1A, 1B). The apical surface of RPE cells lacks

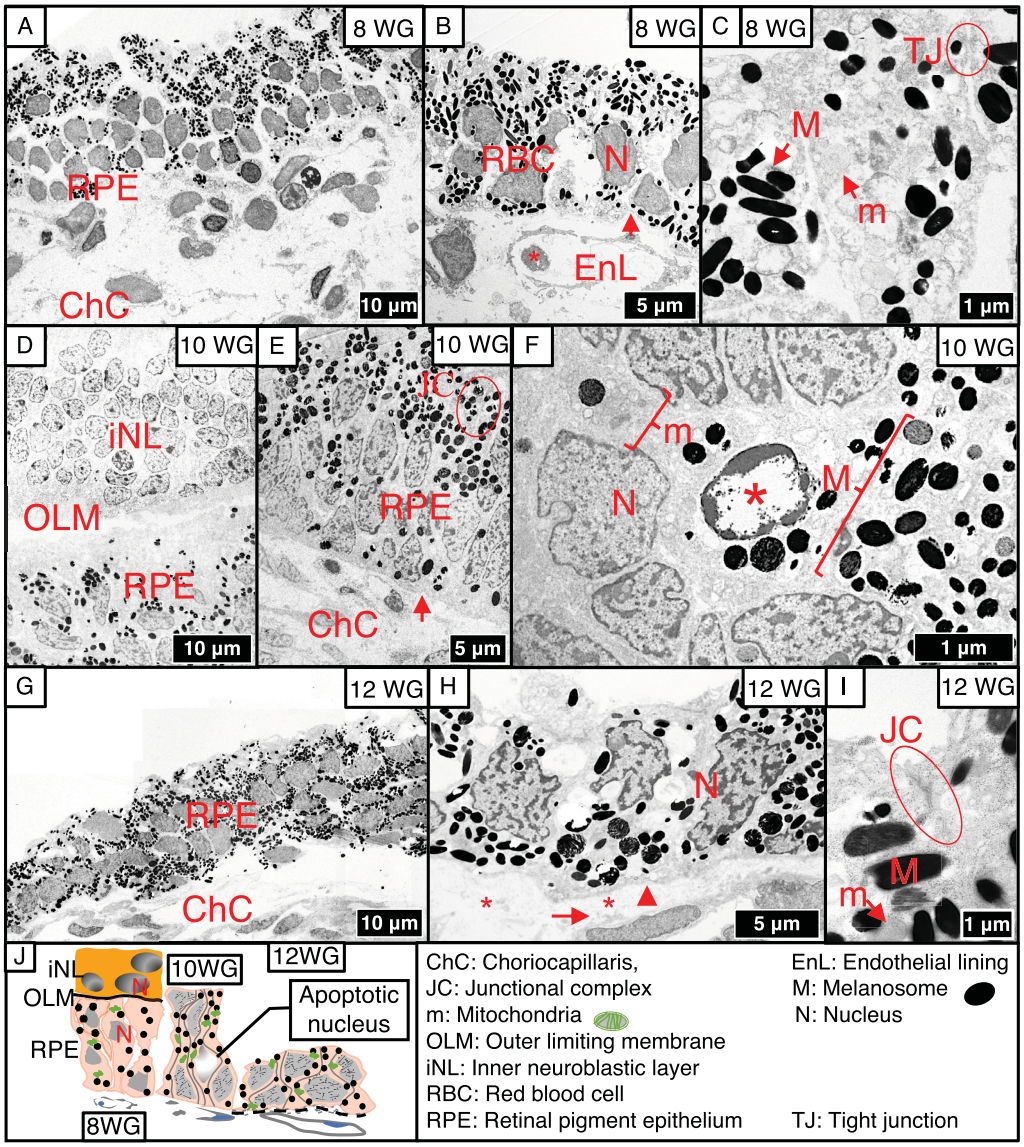

Figure 1. Initial RPE development in first trimester between eight to 12 WG. All data for this study represent observations made on one human specimen per age group. A minimum of 5 fields of view at three levels separated by 50 µm intervals were captured and analyzed for all specimens at each age and location. (**A**) Pseudostratified columnar RPE and primitive ChC evident at eight WG. (**B**) RPE with different levels of nuclei (*N*) containing evenly dispersed chromatin, and primitive endothelial linings (*EnL*) with red blood cell (*asterisk*) evident. *Arrow* is pointing to incipient RPE cell membrane. (**C**) High-magnified view showing primitive apical tight junctions (*TJ*, *circle*), partial attachment of lateral borders, and randomly distributed melanosomes (*M*) and mitochondria (*m*). (**D**) Primitive inner neuroblastic layer (*iNL*) loosely attached to RPE through outer limiting membrane (*OLM*) at 10 WG. (**E**) *Circle* showing development of apicolateral junctional complexes (*JC*), incipient RPE cell membrane (*arrow*), and ChC. (**F**) High-magnified view showing a possible apoptotic nucleus (*red asterisk*) with chromatin margination, surrounded by a group of melanosomes and randomly localized mitochondria. (**G**) Montaged view showing differentiation from pseudostratified epithelia to simple cuboidal layer at 12 WG. (**H**) RPE cell membrane (*vertical arrowhead*), incipient patchy elastic layer (*horizontal arrow*), primitive inner and outer collagenous layers (*red asterisks*) are evident. (**I**) High-magnified view showing apicolateral JC (*circle*). (**J**) Pseudostratified columnar epithelia in association with iNL through OLM at eight WG differentiates to cuboidal epithelium at 12 WG. This summary diagram is based on tracings of actual cells or cell clusters at each developmental stage and were developed to represent a summation of huge numbers of fields of views to show changes in RPE morphology at the whole cell/cell cluster level. Images have been drawn to scale and represent a higher magnification view of cell detail than would have been possible by photographing the TEM thin sections stained with toluidine blue.

microvilli, and there is no evidence of RPE basal lamina (Fig. 1B). The lumen of ChC vessels is often not patent, with only one layer of choroidal vasculature, and no evidence of basal lamina. Adjacent RPE cells are joined by junctional complexes (Fig. 1C).

By 10 WG, the cells remain as pseudostratified columnar RPE (taller). A primitive inner neuroblastic layer is loosely attached to adjacent RPE cells, and an early outer limiting membrane is present (Fig. 1D). The RPE have an identifiable basal lamina (Fig. 1E) and melanosomes (several stages) are present. Organelles remain randomly distributed. Smaller nuclei with clumped marginated chromatin characteristic of apoptosis are present (Fig. 1F), supportive of numerous earlier reports of the overproduction of cells during normal mammalian development, which is subsequently reduced by selective pruning via apoptosis.[32]

The RPE transitions from a pseudostratified-columnar epithelia at eight WG to a simple cuboidal shape by 12 WG, where the RPE cell shape shortens, becoming more cuboidal, and the nuclei are now located at the same level (Fig. 1G). The apicolateral junctional complexes, RPE cell membrane, patchy elastic layer, and primitive inner and outer collagenous layers are evident at this age (Figs. 1H, 1I). At 12 WG, the RPE are simple cuboidal with a reduced area (Fig. 1J).

Significant RPE Interaction With POS and ChC in the Second Trimester Between 16 to 24 WG

At 16 WG, the primitive inner segment of photoreceptors, outer limiting membrane, and inner neuroblastic layer are present (Figs. 2A, 2B). The RPE cell becomes significantly shorter and wider, with apical long microvilli and apicolateral junctional complexes (Fig. 2C). At 20 WG, both the RPE and ChC basal lamina are present (Figs. 2D, 2E). At this age, the choroidal vessels have pericytes and fenestrae (Figs. 2D–F). Outer and inner nucleus layers and amacrine and horizontal cells indicate retinal specialization at 24 WG, with increased mitochondria also present in the inner segment of photoreceptors (Fig. 2G). The RPE show increased mitochondria and melanosomes randomly distributed in the cytoplasm (Fig. 2H).

Organelle Relocation at 26 WG, Coincident With Eye Opening

The upper and lower eyelids are fused at 10 WG. Although there is a variation regarding the events and timing of eyelid separation, it is generally agreed that separation begins around 20 WG[33] and is completed by 26 WG.[34,35] In this study, coincident with eye opening at 26 WG, melanosomes and mitochondria migrate to the apical and perinuclear regions of RPE cells (Figs. 3A, 3B). The quantitative aspects of RPE organelles seen here (Fig. 3C) are consistent with a recent comprehensive quantitative study of human RPE.[36] Organelle distribution between the upper and lower regions of the RPE cells at this age shows that 65% ± 3% of melanosomes are localized apically in the ONH, whereas 46% ± 5% are apically distributed in the mid periphery (Fig. 3D), as previously reported.[36,37]

Characterization of BES at 26 WG

The BES was first observed between basal cell membranes of adjacent RPE cells from 26 WG in the region adjacent to the ONH and in the mid periphery. The BES is characterized as a triangular space delineated by the two cell membranes of adjacent RPE cells and RPE basal lamina (Figs. 4A, 4B). The BES was filled with clear flocculant proteinaceous materials, which are similarly observed in aged specimens (unpublished observation), leading us to suggest that this novel characterization of the BES in normal human RPE differentiation has high functional relevance to the pathogenetic processes of pigment epithelial detachment and dry age-related macular degeneration (AMD).

Phagocytosis Is Evident Coincident With Eye Opening at 26 WG

The first evidence of phagosomes and complex granules at 26 WG slightly increases by 36 WG (not significant). The average area of melanosomes significantly decreases between six to 17 years, whereas the area of complex granules significantly increases at the same time (Table 1). The area of phagosomes per cell increases significantly as a function of age after birth (6–17 years) (Table 1). The average area of mitochondria increases between eight to 24 WG (not significant), followed by significant increases coincident with eye opening at 26 WG, followed by another increase between six to 17 years, which is significantly different from that seen at 26 WG (Table 1).

Autophagy Is Evident From 32 WG

At 32 WG, RPE cells have fully mature apicolateral junctional complexes sealing the surface and strengthening the integrity of the RPE layer (Fig. 5A). This is the first age where we observed the definitive ultrastructural evidence of autophagosomes and mitophagosomes as double membrane-bound structures (Figs. 5B, 5C). These structures are present in the perinuclear and basal portion of the RPE and are responsible for recycling of damaged organelles (Figs. 5D, 5E).[38,39] Mitophagosomes (Figs. 5B, 5C) and mitolysosomes (Fig. 5E), with cristae and vesicles enclosed in an intact membrane are clearly distinguished from oval-shaped mitochondria with visible cristae (Fig. 5E). RPE cells demonstrate functional maturation including organelles associated with heterophagic and autophagic processes, apicolateral junctional complexes, and BES at 36 WG (Figs. 5F, 5G). At this age, RPE basal cell membrane infoldings are present (Fig. 5E). Mitochondrial accumulation in basal and lateral regions of RPE cells adjacent to the BES is observed (Fig. 5F). The POS discs' phagocytosis and phagosome are evident adjacent to the apicolateral junctional complexes (Fig. 5H). Between six to 17 years, there are no significant changes in areas of autophagy, mitophagic organelles, and mitochondria (Table 1).

Lipofuscin Formation and Exocytosis to the BES Is Evident at Six Years

Lipofuscin granules were observed at six years (Figs. 6A–C). These round to oval, single-membrane–bound granules have been reported in older eyes[40] and are present in the mid and basal portions of RPE cytoplasm from six years and exocytosed into the BES (Fig. 6C). The average area of these indigestible byproducts slightly increased at nine years and significantly increased at 17 years (Table 1).

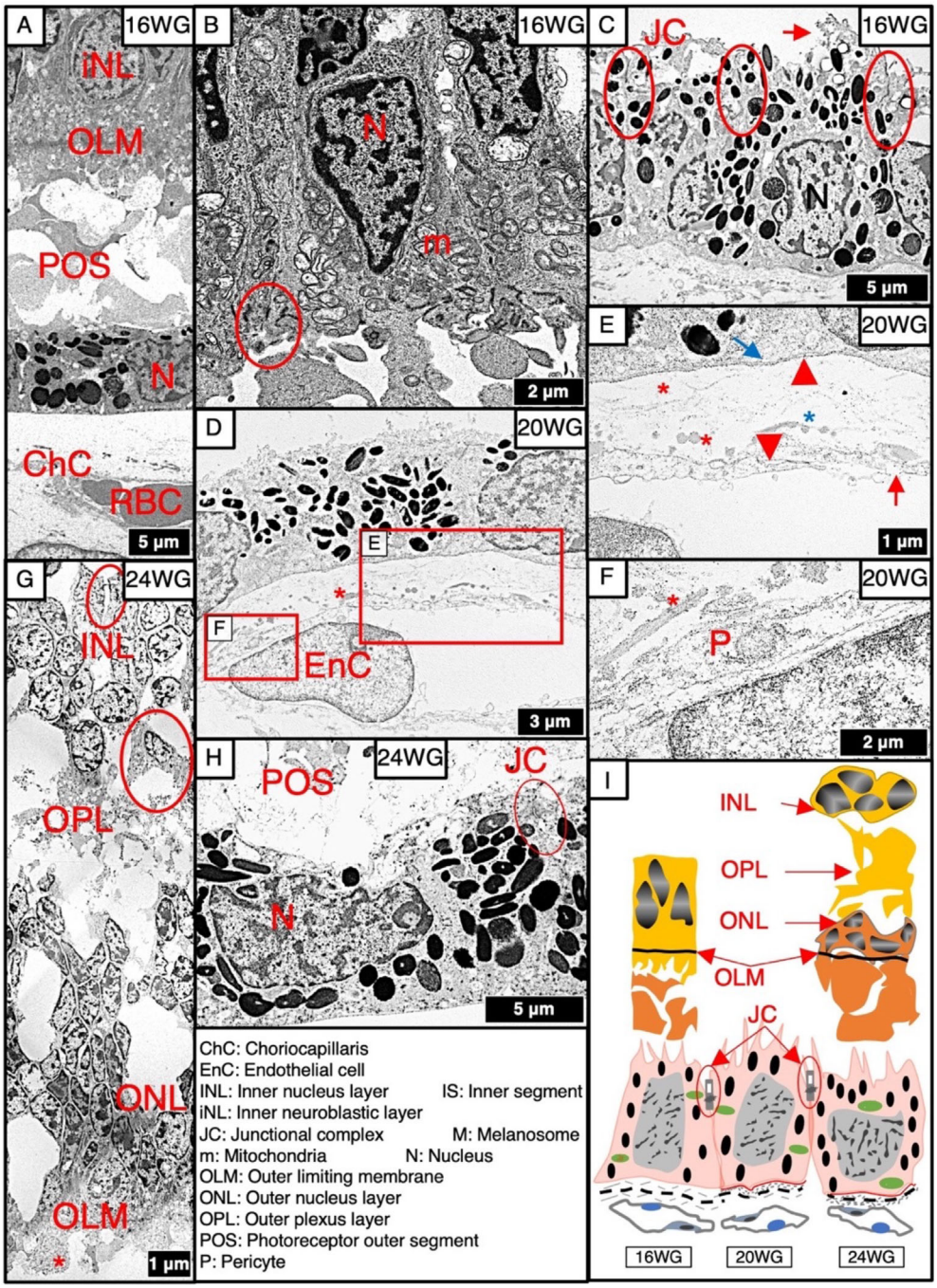

Figure 2. RPE interact with POS and choriocapillaris in second trimester between 16 to 24 WG. One specimen per age was examined throughout this study where five fields of view at three levels separated by 50 µm were examined per specimen. Cellular enlargement, apicolateral specialization, and incipient formation of underlying BrM are evident. (**A**) The nuclei (*N*) of primitive cells of the inner neuroblastic layer (*iNL*), outer limiting membrane (*OLM*), and underlying primitive POS are evident at 16 WG. (**B**) Developing iNL contains nuclei of outer nucleus layer (*ONL*), large number of mitochondria (*m*), and tight junctions between adjacent cells (*circle*). (**C**) Apical development of RPE with microvilli (*horizontal arrow*) and junctional complexes (*JC*) (*circles*) evident. (**D**) Melanosomes randomly located in the cytoplasm, patchy elastic layer (*red asterisk*), and endothelial cells evident at 20 WG. Representative regions in *boxes* are shown in **E** and **F**. (**E**) RPE cell membrane (*blue arrow*), RPE and choroidal basal lamina (*red arrowheads*), inner and outer collagenous fibers (*red asterisks*), elastic layer (*blue asterisk*), and fenestration toward RPE (*red arrow*) evident. Basal infoldings are not present at this early age. (**F**) Elastic layer (*asterisk*) and pericyte (*P*) are shown. (**G**) Montaged view showing development of iNL including ONL, outer plexiform layer, amacrine and horizontal cells (*circles*) in proximal and distal areas of the inner nucleus layer (*INL*) at 24 WG. Accumulation of mitochondria (*asterisk*) evident beyond the OLM in primitive inner segment of photoreceptors. (**H**) Primitive POS, JC (*circle*), and localization of organelles evident. (**I**) Schema showing no significant change in cell width from 16 to 24 WG.

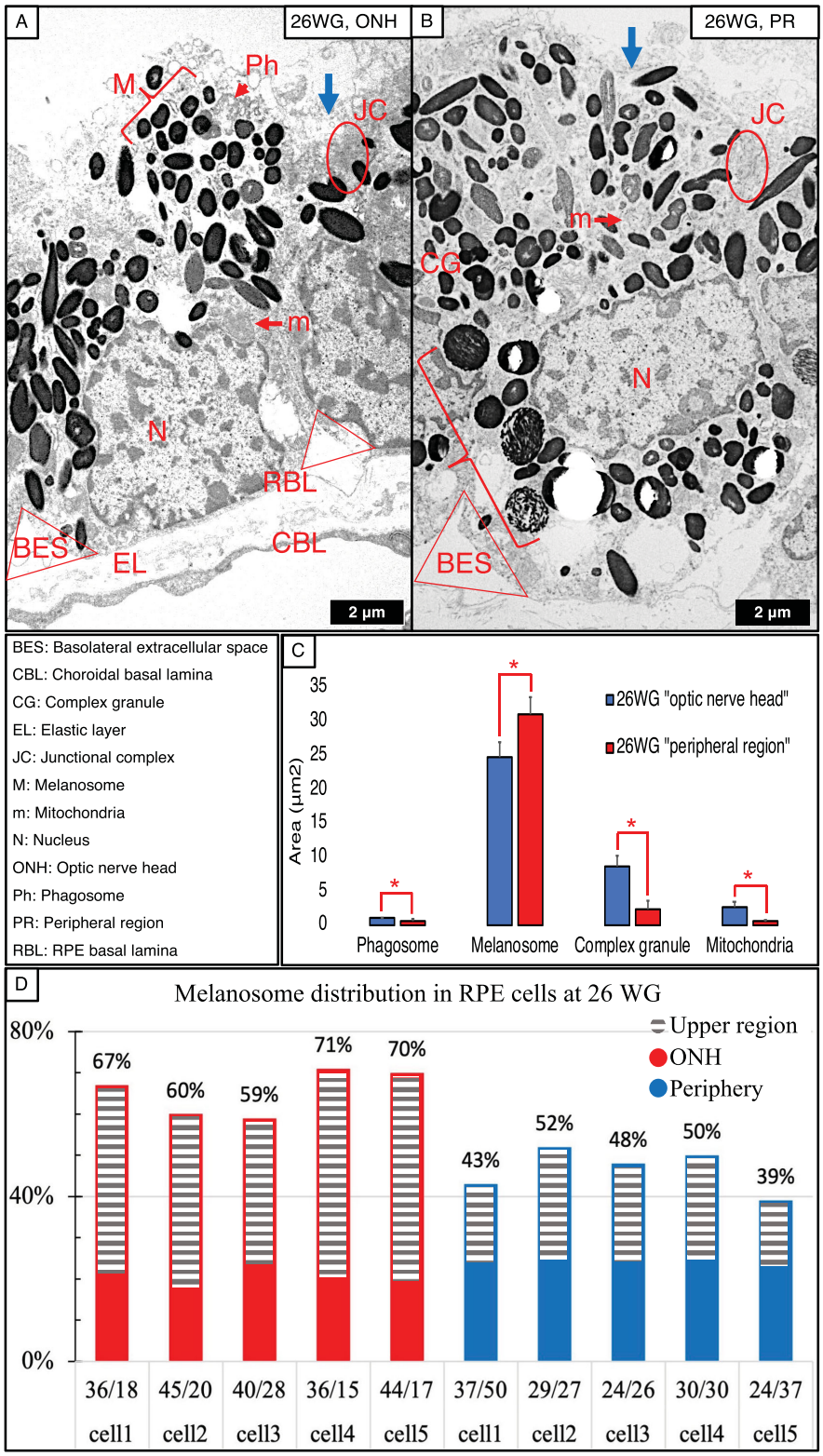

Figure 3. Organelle relocation at 26 WG, coincident with eye opening. *Circles* show junctional complexes (*JC*) between adjacent RPE cells. Apical-basal redistribution of RPE organelles occurs sooner in the region adjacent to the ONH than in the peripheral region (*PR*). (**A**) Shows human RPE at 26 WG in the region adjacent to the ONH. Apical microvilli (*blue arrow*) and phagosome (*Ph*) are evident. Melanosomes (*M*, *bracket*) migrate to the apical region, and mitochondria (*m*) are localized in the perinuclear region (*red arrow*). Elastic layer (*EL*), RPE basal lamina (*RBL*), choroidal basal lamina (*CBL*), and BES are evident. (**B**) In contrast, apical microvilli (*blue arrow*), melanosomes, and mitochondria are located randomly in RPE cells from the periphery of a 26 WG specimen indicative of a disc to peripheral topography of RPE maturation. Group of large spherical melanosomes (*bracket*) are in the basolateral region. (**C**) Semiquantitative ultrastructural analysis demonstrates the average area of phagosomes, complex granules, and mitochondria in the region adjacent to the ONH is significantly greater than in the PR at 26 WG ($P < 0.05$). Accompanied with these changes, melanosomes occupy a larger area in the peripheral region compared

Investigative Ophthalmology & Visual Science

to the region adjacent to the ONH. (**D**) More than 65% ± 3% of melanosomes localized apically in the region adjacent to the ONH, whereas 46% ± 5% are apically distributed in the mid periphery region. Melanosome distribution in RPE cells at 26 WG is expressed as mean ± SEM, per RPE cell.

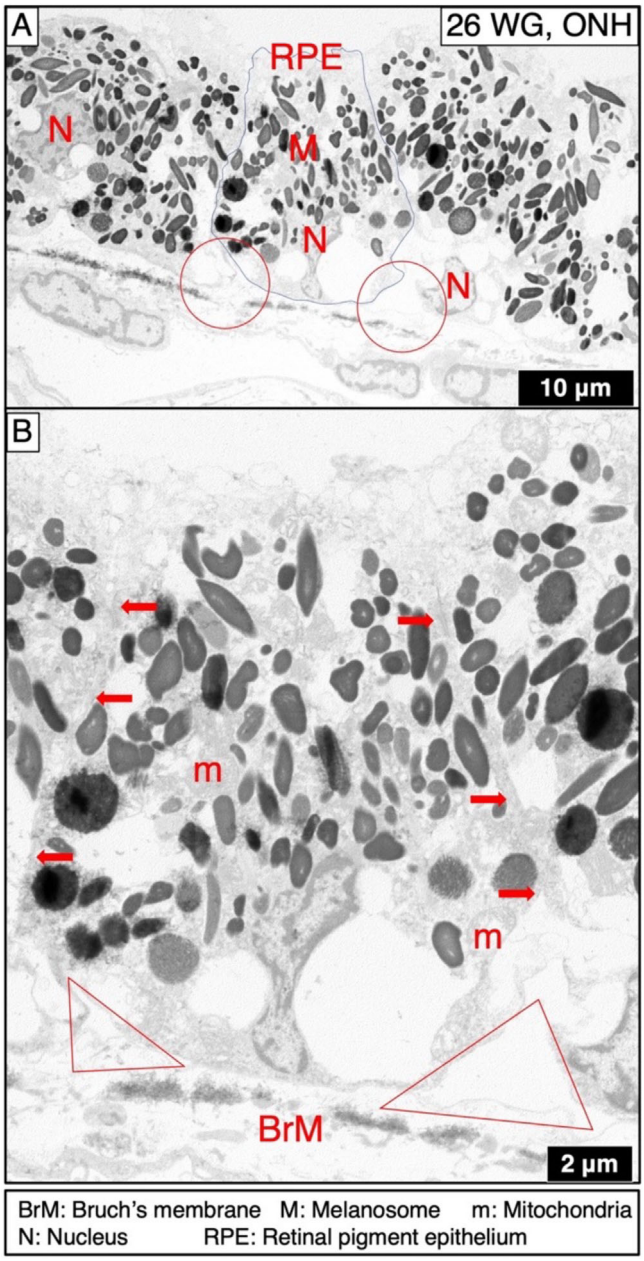

Figure 4. Characterization of BES at 26 WG, coincident with eye opening. (**A**) *Circles* show BES between adjacent RPE cells with different levels of nuclei (*N*). Melanosomes (*M*) migrate to the apical region. (**B**) The high magnified view shows the BES as a triangular space along the lateral border of RPE cells (*arrows*) delineated by the two cell membranes of adjacent RPE cells and RPE basal lamina of BrM. Mitochondria (*m*) are localized in the perinuclear region.

RPE and ChC Maturation Follow Central to Peripheral Topography of Maturation

We demonstrate that the mitochondria and complex granules areas per cell in the ONH are significantly greater than in the mid periphery, coincident with eye opening at 26 to 28 WG (Fig. 3C, Table 1). Similarly, the average area per RPE cell is substantially greater in a region adjacent to the ONH when compared to the mid periphery at 26-28 WG (Table 2). RPE cells were found to be taller in the region adjacent to the ONH when compared to the mid periphery at 26-28 WG (Table 2). When approaching the peripheral RPE from the ONH, cells appear to be shorter with less development at the same timepoint, as evidenced by reduced phagocytosis (Table 1). The ChC vessels were poorly developed with vascular precursor endothelial cells as the only vascular elements evident at 8 WG. Consistent with our earlier report,[28] a rapid maturation of the choroidal vasculature occurs, as evidenced by formation of fully developed fenestrated choroidal capillaries with a basal lamina and pericytes at 20 WG. The number of fenestrae of capillaries were counted, and the thickness of endothelial basal lamina was measured toward RPE and scleral sides. The thickness of endothelial cell basal lamina was observed to be greater toward RPE when compared to the scleral side in both the ONH and mid periphery, and significantly greater in the mid periphery when compared to the ONH (Fig. 7A). The number of fenestrae were more frequent on the RPE side when compared to scleral side in both the ONH and mid periphery but with higher frequency in the ONH when compared to the mid periphery (Fig. 7B) ($P < 0.05$).

Nuclear Area Decreases Before 36 WG, Whereas RPE Cell Area Continues to Increase

The nucleus area relative to total cytoplasmic area (N/C ratio) increases significantly between eight to 10 WG, then significantly decreases by 26 WG, coincident with eye opening, and plateauing thereafter (Fig. 8A, Table 2). RPE transition from pseudostratified columnar (eight WG) to simple cuboidal (12 WG) and then to simple squamous (wider than their height relative to the basal lamina) (16 WG). There is a significant increase in the cell height at 26 WG, with cells returning to a simple columnar shape (Fig. 8B). The cell morphology progressively transitions back to a simple cuboidal shape at 32 WG and then simple squamous by 36 WG ($P < 0.05$). There are no further significant changes in shape or dimension between six to 17 years (Table 2).

Development of BrM in the Second Trimester Toward 20 WG

The BrM consists of apolipoproteins (A–E), members of the complement system (factor H, complement 3, lectin, complement component 8-9), trace elements, lipofuscin, and autophagic byproducts, and the majority of BrM is derived from choroidal stroma.[41] A primitive BrM consisting of a patchy elastic layer with inner and outer collagenous fibers is present from 12 WG (Fig. 1H). At this age, the RPE and ChC lay down collagenous fibers onto the elastic layer of BrM, forming the primitive inner and outer collagenous layers. BrM further develops as RPE, and choroidal endothelial cells form the outermost layers known as basal lamina at 20 WG (Figs. 2D, 2E). The thickness of BrM increases significantly

Table 1. Raw Data of Ultrastructural Measurement of RPE Cells in Human Eye Samples

Age	M (μm²)	Ph (μm²)	CG (μm²)	m (μm²)	aPh/aLy (μm²)	mPh (μm²)	Lf (μm²)
8 WG	9.66 ± 1.56	0	0	0.28 ± 0.07	0	0	0
10 WG	10.36 ± 0.68	0	0	0.34 ± 0.34	0	0	0
12 WG	14.06 ± 3.87	0	0	0.20 ± 0.10	0	0	0
16 WG	13.30 ± 3.34	0	0	0.37 ± 0.37	0	0	0
20 WG	15.22 ± 1.50	0	0	0.36 ± 0.19	0	0	0
24 WG	24.25 ± 2.07	0	0	0.29 ± 0.21	0	0	0
26 WG (adjacent to the ONH)	24.73 ± 0.93	0.97* ± 0.12	8.62* ± 1.59	2.60* ± 0.75	0	0	0
26 WG (Periphery)	30.92 ± 1.70	0.50 ± 0.05	2.35 ± 1.18	0.62 ± 0.15	0	0	0
28 WG (adjacent to the ONH)	26.60* ± 0.90	1.10* ± 0.26	8.34* ± 0.60	1.81* ± 0.87	0	0	0
28 WG (Periphery)	20.09 ± 3.12	0.20 ± 0.10	5.19 ± 0.75	0.56 ± 0.27	0	0	0
32 WG	26.12 ± 1.69	1.18 ± 0.56	9.34 ± 1.65	2.68 ± 0.08	0.27 ± 0.05	0.23 ± 0.06	0
36 WG	27.00 ± 2.15	1.22 ± 0.04	9.28 ± 2.02	3.36 ± 0.66	0.25 ± 0.04	0.25 ± 0.04	0
6 Y	10.40* ± 1.49	3.03* ± 0.52	20.99* ± 0.89	4.20* ± 0.51	0.27 ± 0.04	0.26 ± 0.02	3.41 ± 0.63
9 Y	10.31 ± 0.64	3.62 ± 0.89	25.61 ± 2.67	4.21 ± 0.53	0.36 ± 0.05	0.25 ± 0.01	3.65 ± 0.30
17 Y	11.37 ± 1.66	3.18 ± 0.49	23.18 ± 1.19	4.96 ± 0.39	0.41 ± 0.07	0.24 ± 0.02	8.20* ± 0.59

aPh, autophagosomes; aLy, autolysosomes; CG, complex granules; Lf, lipofuscin; m, mitochondria; M, melanosomes; mPh, mitophagosomes; Ph, phagosomes.

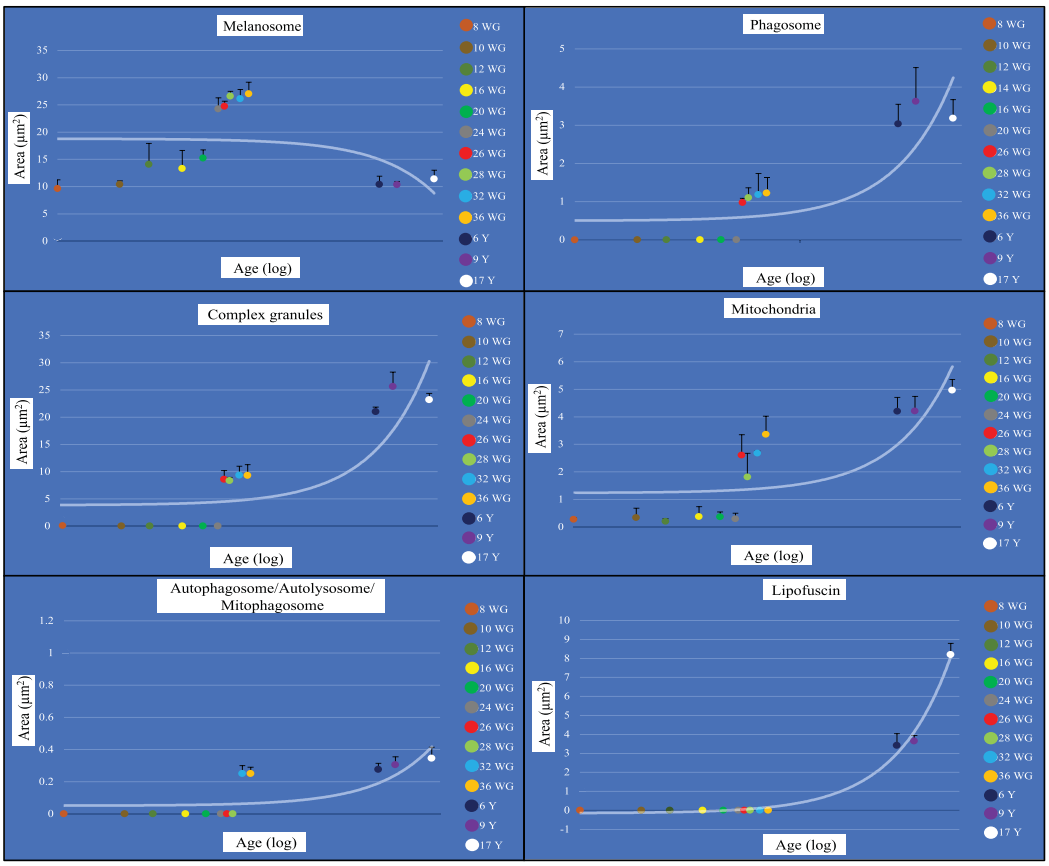

A composite figure plate showing graphical representations of each of the organelles quantified as a function of age in a logarithmic x axis. A semiquantitative analysis performed by using iTEM software. The mean ± SEM of repeated measures in 5 fields of views on one specimen for each age were analyzed by using a one-way ANOVA with post-hoc tests for analysis, and $P < 0.05$ was considered significant. The number and area (μm²) of M, Ph, CG, m, aPh, aLy, and mPh measured in low-magnification (<8000) and high-magnification images (20,000–60,000). The area of ultrastructural changes coincident with eye opening at 26 WG. Except melanosomes at 26 WG, the average area occupied by RPE organelles in the region adjacent to the ONH was significantly greater than in the peripheral region at 26–28 WG. The increasing trend of melanosome area significantly reverses after birth, whereas the area of phagosomes and complex granules, which are characterized from 26 WG, increases significantly after birth. The area of mitochondria increases significantly at 26 WG and continues thereafter. The area of Lf at six years slightly increases at nine years and significantly increase at 17 years. All parameters were quantified in both the regions adjacent to the ONH and mid-peripheral retina at 26 WG and 28 WG to determine whether, like other measures of retinal development, there was a clear disc to periphery topographical maturation of human RPE.

* $P < 0.05$.

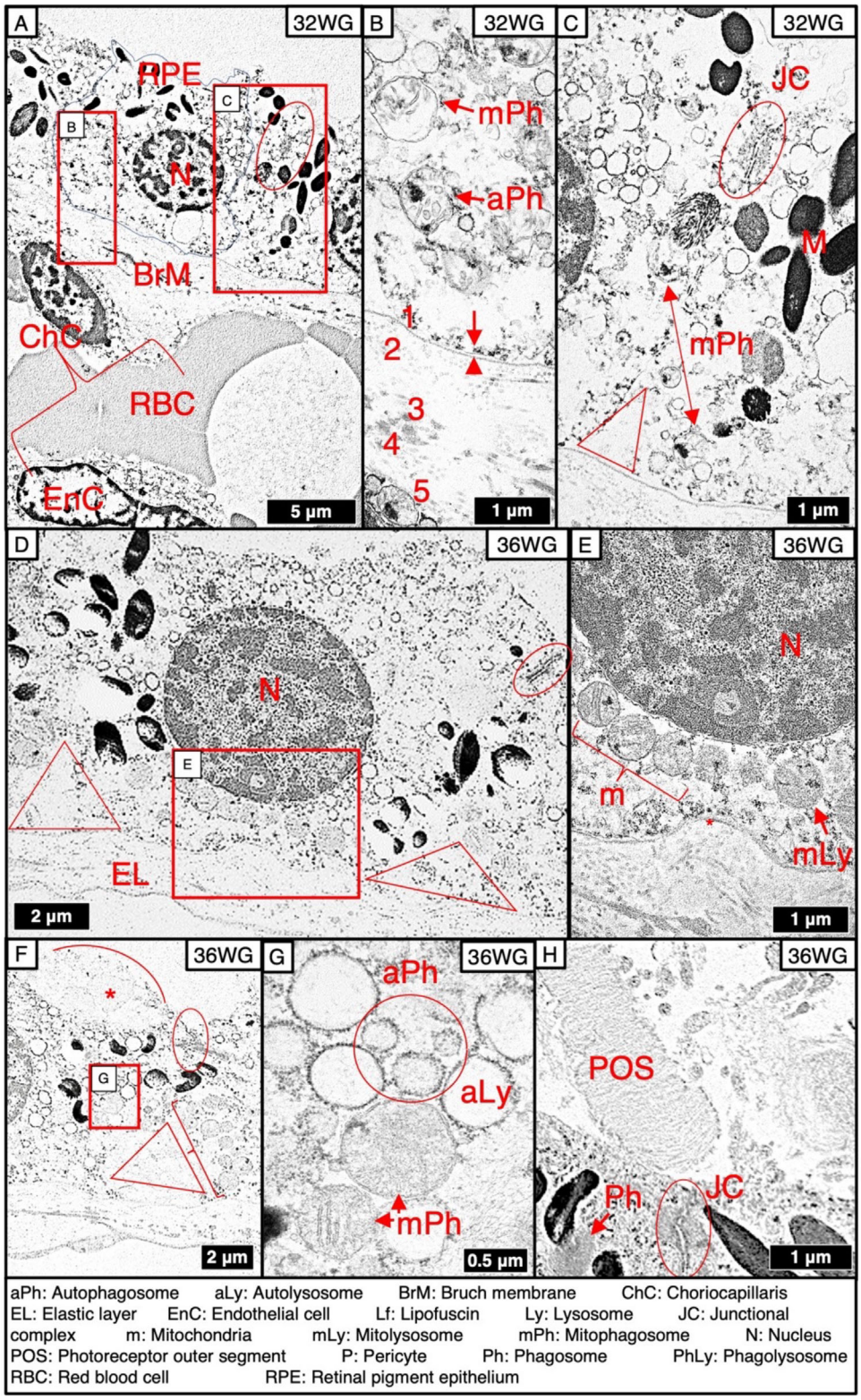

Figure 5. Autophagy and mitophagy evident from 32 WG. (**A**) RPE and BrM evident at 32 WG. Red blood cells and endothelial cells (*EnC*) are visible in the ChC. Representative regions in boxes are shown in **B** and **C**. (**B**) High-magnified montage showing mitophagosome (*mPh*) and autophagosome (*aPh*). A well-characterized BrM is evident at this age because all its layers are discernible; RPE basal lamina (1), inner collagenous (2), elastic (3) outer collagenous (4) and choroidal basal lamina (5). (**C**) Circle shows apicolateral junctional complexes (JC). Melanosomes (M) and mitophagosome evident in the RPE cytoplasm adjacent to the basolateral border of RPE cells. Triangle shows the BES between adjacent RPE cells. (**D**) The JC (*circle*) and BES (*triangles*) delineate the apicolateral and basolateral borders of adjacent RPE cells at 36 WG. Representative region in box is shown in **E**. (**E**) Basal infoldings of RPE cell membrane (*asterisk*), mitochondria (*bracket*), and mitolysosomes (*mLy*) are evident. (**F**) Low-magnified view showing outer segment discs (*asterisk*) surrounded by apical microvilli (*curve*),

JC (*circle*), mitochondria (*bracket*), and adjacent BES (*triangle*). Representative region in box is shown in **G**. (**G**) Various structures showing autophagosomes (*circle*), autolysosome (*aLy*), late (*top-right*) and early (*bottom-left*) mitophagosomes. (**H**) Photoreceptor outer segment discs recognized for phagocytosis and phagosome (*Ph*) evident adjacent to the apicolateral JC.

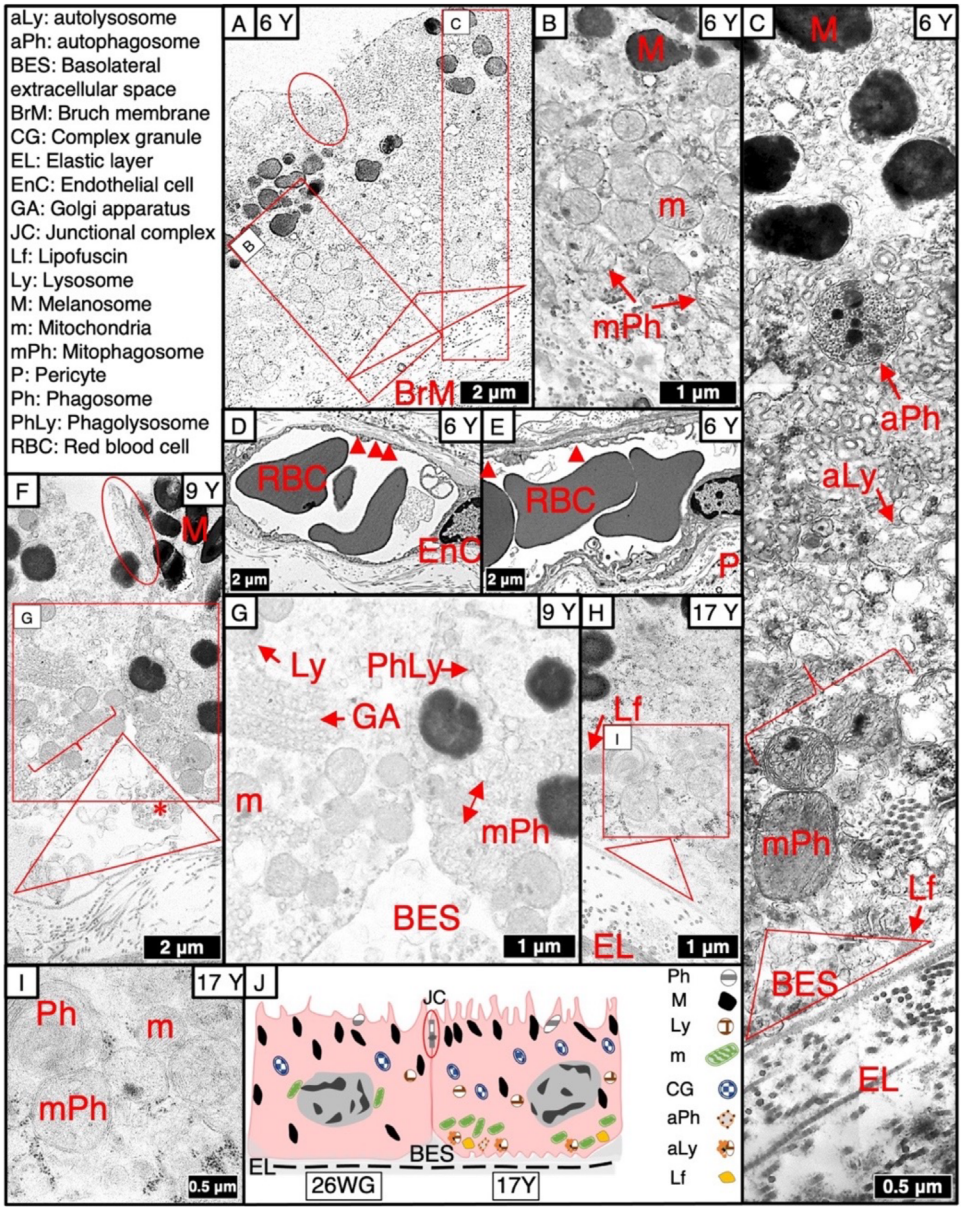

Figure 6. Lipofuscin formation and exocytosis to the BES evident at six years. (**A**) The apicolateral junctional complexes (*oval*) and the BES (*triangle*) and underlying BrM are evident at six years. Boxes are represented in **B** and **C**. (**B**) Montaged view showing apical melanosomes (*M*), mitochondria (*m*), and mitophagosomes (*mPh*) in the basolateral region. (**C**) Autophagosome (*aPh*), autolysosome (*aLy*), and mitophagosomes (*mPh*) (*bracket*) are evident. Lipofuscin (*Lf*) exocytosed into the BES. (**D, E**) The representative images delignated the number of fenestrae (*red solid triangles*) in the choriocapillaris towards the RPE adjacent to the optic nerve head (**D**) and peripheral region (**E**). Red blood cells (*RBC*, *stars*), endothelial cells (*EnC*) extension surrounding the lumen, and pericyte (*P*) are evident. (**F**) Junctional complexes (*circle*), melanosomes, and mitochondria (*bracket*) adjacent to the basolateral border of RPE, and BES containing autophagic byproducts (*asterisk*) are evident at nine years. Mitochondria and mitophagosomes localized in the basolateral region adjacent to BES (*triangle*). (**G**) The phagolysosome (*PhLy*), Golgi apparatus (*GA*), lysosome (*Ly*), and autophagic byproduct deposition into the BES are evident. Mitochondria and mitophagosomes localized in the basolateral region adjacent to BES. (**H**) Lipofuscin granule evident adjacent to the BES (*triangle*) at 17 years. *Box* is shown in **I**. (**I**) Phagosome (*Ph*), mitochondria, and mitophagosome are characterized in high magnification view. (**J**) Schematic in which the left panel (26 WG) shows a cell with distinct apical melanosomes and perinuclear mitochondria development with the evidence of phagosome and complex granules formation at 26 WG. There is no evidence of drusen formation at this age. The *right panel* (17 years) shows a fully functional RPE cell. Mitochondria distribute adjacent to basal infoldings and in the vicinity of the BES, the site of byproducts deposition.

Table 2. Measurement of RPE Dimensions in Human Eye Samples

Age	Height (μm)	Width (μm)	Cell Area (μm^2)	Cytoplasm (μm^2)	Nucleus (μm^2)	N/C Ratio (%)
8 WG	17.31 ± 0.08	4.46 ± 0.05	77.17 ± 1.22	62.83 ± 1.79	14.34 ± 2.70	23 ± 5
10 WG	20.76 ± 0.40	4.02 ± 0.60	83.70 ± 3.07	55.36 ± 6.11	28.34 ± 3.52	54* ± 7
12 WG	9.53* ± 0.30	6.33 ± 0.30	60.12 ± 1.68	44.36 ± 7.16	23.35 ± 5.68	53 ± 8
16 WG	7.48 ± 0.40	12.13* ± 1.35	89.70 ± 5.46	60.63 ± 6.34	29.07 ± 2.44	49 ± 7
20 WG	7.07 ± 0.24	13.17 ± 0.79	93.04 ± 6.06	65.55 ± 7.32	27.46 ± 3.86	44 ± 9
24 WG	7.35 ± 0.34	15.86 ± 0.13	116.51 ± 3.00	84.25 ± 8.38	32.26 ± 6.78	41 ± 8
26 WG (adjacent to the ONH)	16.14* ± 0.55	9.65 ± 0.39	155.34* ± 2.48	123.16 ± 5.47	32.18 ± 3.86	26* ± 4
26 WG (Periphery)	14.07 ± 0.75	10.00 ± 0.54	140.37 ± 6.98	124.41 ± 12.52	20.96 ± 2.77	17 ± 2
28 WG (adjacent to the ONH)	12.10 ± 0.73	9.39 ± 0.16	113.48* ± 5.79	95.96 ± 5.70	17.52 ± 0.10	18 ± 1
28 WG (Periphery)	11.14 ± 1.28	8.98 ± 0.71	98.35 ± 5.98	77.60 ± 6.27	16.77 ± 2.28	22 ± 1
32 WG	11.54 ± 1.10	11.32 ± 0.46	130.85 ± 8.27	109.83 ± 7.85	21.03 ± 0.43	19 ± 1
36 WG	10.25 ± 0.50	13.43* ± 0.15	137.51 ± 5.21	114.30 ± 5.09	23.21 ± 0.40	20 ± 1
6 years	9.63 ± 0.18	14.95 ± 0.70	144.34 ± 9.05	119.75 ± 7.90	24.59 ± 2.69	21 ± 2
9 years	10.59 ± 0.12	14.82 ± 0.18	156.84 ± 1.13	132.25 ± 1.15	24.60 ± 0.11	19 ± 1
17 years	10.41 ± 0.21	15.26 ± 0.21	158.91 ± 4.31	134.40 ± 5.00	23.50 ± 2.13	18 ± 2

A semi-quantitative analysis was performed by using iTEM software. The mean ± SEM of all measurements for each different age were analyzed by using a one-way ANOVA with post-hoc tests for analysis, and $P < 0.05$ was considered significant. The height, width (μm), cytoplasm, nucleus, and cell area (μm^2) were measured. RPE cell dimensions at eight WG increased at 10 WG and significantly decreased at 12 WG. Coincident with eye opening at 26 WG, RPE cells become significantly taller. The average cell area is substantially greater in the region adjacent to the ONH when compared to the peripheral region at 26 to 28 WG. RPE cells become wider at 36 WG ($P < 0.05$), with no further significant change in dimensions thereafter. The nucleus area relative to total cytoplasmic area (N/C ratio) increased significantly between eight to 10 WG but decreased by 26 WG and plateaued thereafter.

*$P < 0.05$.

from 36 WG to six years, with no change up to 17 years (Fig. 9).

Discussion

Formation of tight junctions in the apicolateral region (10 WG) and development of junctional complexes along the lateral border of adjacent RPE (12 WG) are necessary for the RPE to transition to a simple cuboidal epithelium. Each adjoining RPE cell contributes to the formation of an assembly of closed connexin hemichannels developing into large intracellular channels of gap junctions.

Development of apicolateral junctional complexes is critical in stabilizing the RPE layer as the eye grows. In this study, initial junctional complexes from 10 WG are fully developed by 16 WG. Efimova and Svitkina[42] proposed that the actin cytoskeleton at junctions and desmosomes act as a dynamic

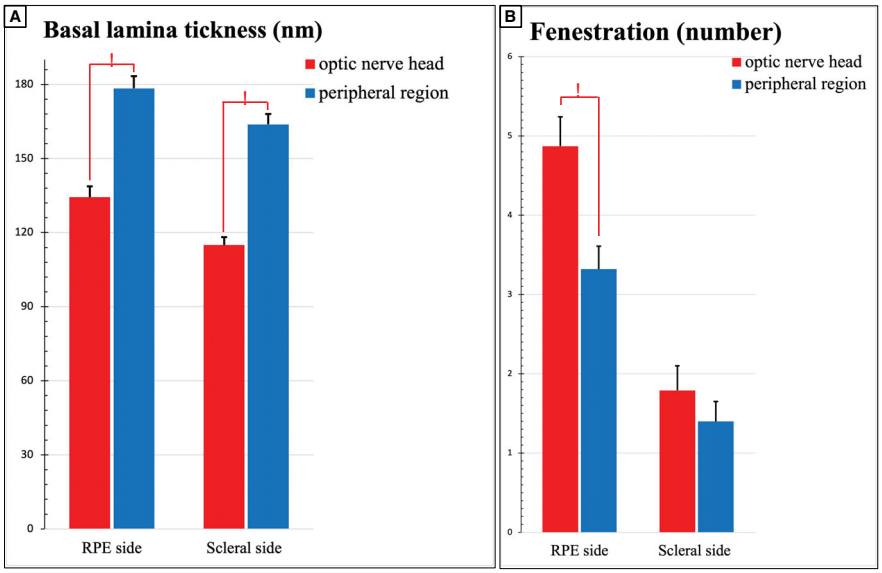

Figure 7. ChC maturation follows central to peripheral topography of development. A semi-quantitative analysis was performed by using iTEM software. The mean ± SEM of all measurements for each five different areas of 25 capillaries at six years in high-magnification images (20,000–60,000) were analyzed by using a one-way ANOVA with post-hoc tests for analysis, and $P < 0.05$ was considered significant. (**A**) Thickness of the endothelial cell basal lamina was observed to be greater toward RPE when compared to the scleral side in both region adjacent to the ONH and peripheral region and significantly more in the peripheral region when compared to the region adjacent to the ONH. (**B**) The number of fenestrae in the ChC are significantly greater toward the RPE cells when compared to the scleral side in both region adjacent to the ONH and periphery and significantly more in the region adjacent to the ONH when compared to the peripheral region. Data are expressed as mean ± SEM, per RPE cell.

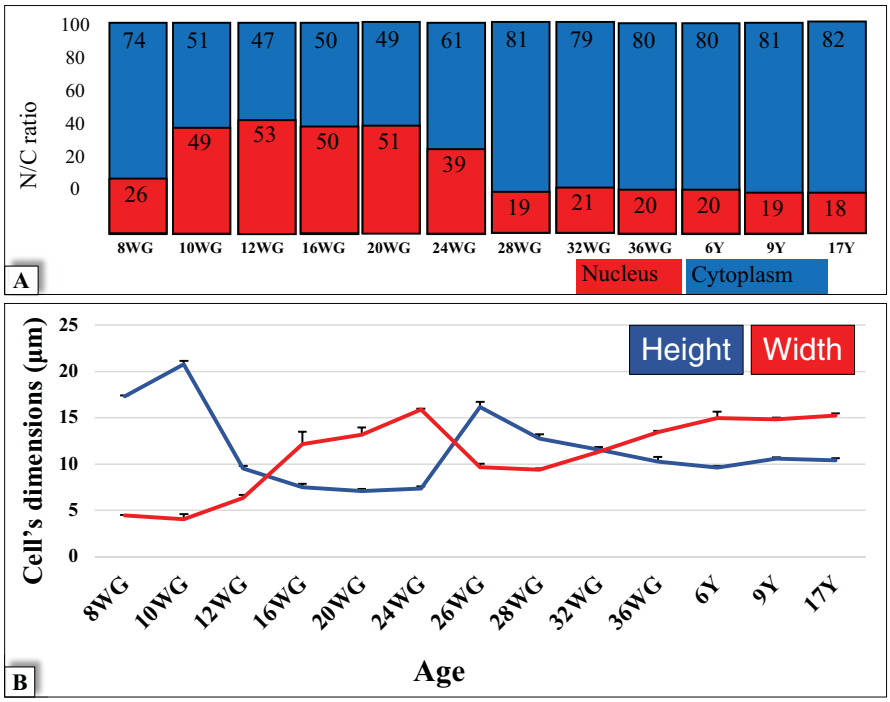

Figure 8. Nuclear to cytoplasm ratio changes during pigment epithelial development. (**A**) The column chart represents the increase in nucleus area relative to total cytoplasmic area (*N/C*) ratio between 10 to 20 WG, followed by a significant decrease by 28 WG, and plateau after birth. (**B**) RPE height exceeds width significantly (8–12 WG) coinciding with a significant increase in the N/C ratio ($P < 0.05$). From 16 WG, cell width exceeds height to the later stages of development, with the exception at 26 WG (coinciding with eye opening) and 32 WG (both width and height are approximately equal). This morphological change is coincident with the significant decrease in N/C ratio to a lower level than seen at 8 WG, suggesting increased emphasis on the number and distribution of various organelles during the later period of development. The nuclear to cytoplasm ratio is expressed as mean ± SEM at each age where 10 cells were measured at each age.

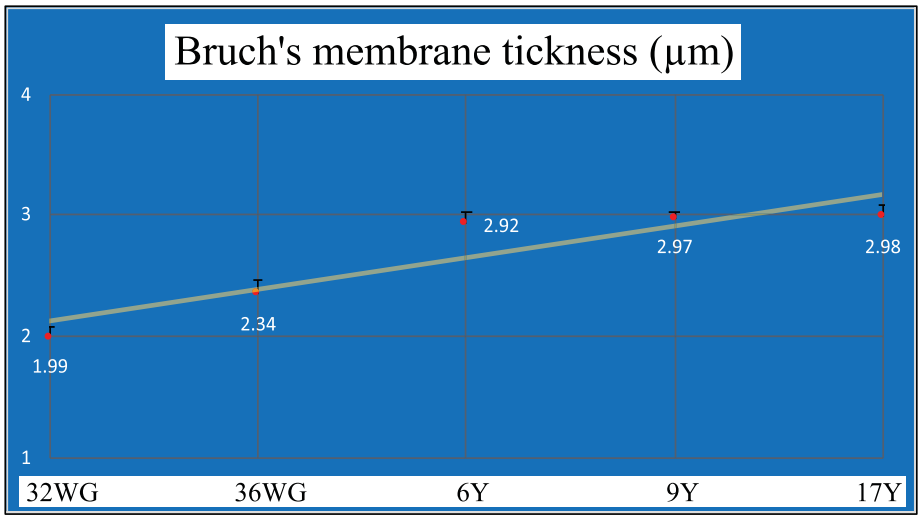

Figure 9. Thickness increasing of BrM through aging. The thickness of BrM was not assessed before 32 WG because it was incomplete. The thickness of BrM increases from 36 WG to six years, with no obvious change up to 17 years. There is a substantial increase in the thickness of BrM from six years, and this increases further as a function of age. Although there was clearly a trend of increasing BrM thickness because of the small sample size, no statistical analyses were undertaken. The thickness of Bruch's membrane is expressed as mean ± SEM, at each age where 10 cells were measured at each age.

push/pull system, wherein pulling forces stabilize intracellular adhesion complexes. Being a postmitotic cell, the RPE is unable to multiply through mitosis to cater for the expansion of the eye globe during development; therefore it relies solely on an increase in cell width as shown in this study where RPE cells become significantly wider between 12 to 24 WG. Consistent with the developmental phenomenon of cellular overproduction followed by selective "pruning" or

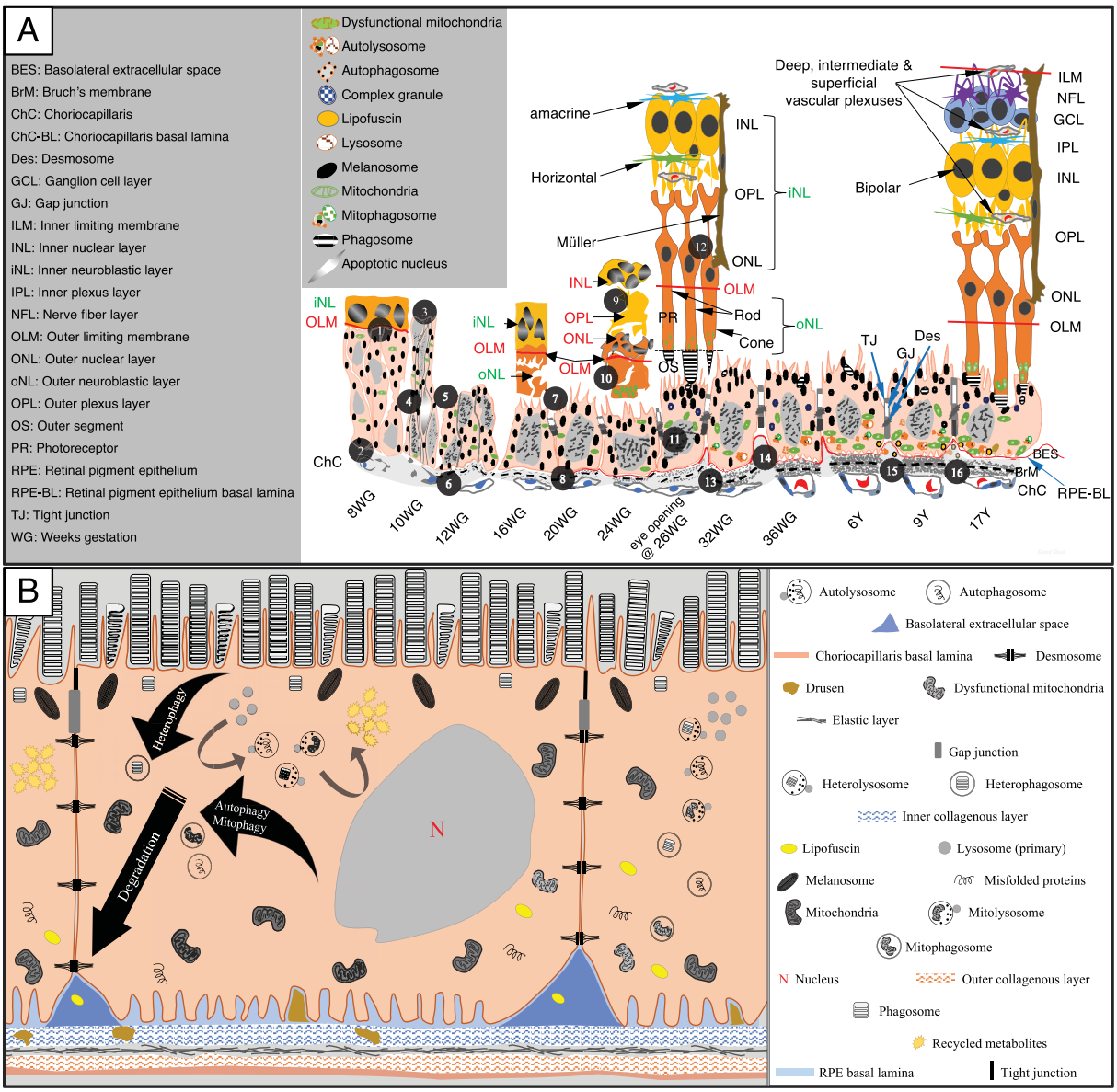

Figure 10. (**A**) The schema details the 16 key ultrastructural morphological stages in the maturation of human retinal pigment epithelial cells from early fetus to adolescence. The inner neuroblastic layer (*iNL*), outer neuroblastic layer (*oNL*), RPE, BrM, and ChC development are evident. (1) The iNL is loosely attached to the pseudostratified columnar RPE through the outer limiting membrane (OLM). (2) RPE cell membrane and primitive vessels with a layer of endothelial cells in ChC is evident at eight WG. (3) Formation of junctional complexes (*JC*) evident from 10 WG. (4) Apoptotic nucleus evident from 10 WG. (5) Simple cuboidal RPE and development of apicolateral JC evident at 12 WG. (6) Inner, outer collagenous fibers and elastic layer of BrM evident from 12 WG. (7) RPE maturation evident by interaction of apical microvilli with primitive photoreceptors in the oNL and a mature apicolateral JC at 16 WG. (8) Formation of RPE, and endothelial cell basal lamina and pericyte evident at 20 WG. (9) Development of iNL including OLM, outer nucleus layer (*ONL*), outer plexiform layer (*OPL*), and inner nucleus layer (*INL*) evident at 24 WG. (10) Accumulation of mitochondria in primitive photoreceptor inner segments (*IS*) and random distribution of RPE organelles are evident at 24 WG. (11) Coincident with eye opening, distinct apical and perinuclear redistribution of melanosomes and mitochondria, phagocytosis, and BES are evident at 26 WG. (12) The oNL consisting of the presumptive POS with differentiated iNL (including amacrine, *horizontal*, and Mu¨ller cells) is evident by 26 WG. (13) Autophagy, mitophagy, and well-characterized BrM evident at 32 WG. (14) Basal infoldings of RPE cell membrane are evident at 36 WG. (15) Lipofuscin and mitochondrial basolateral re-distribution evident at six years. Adjacent RPE cells are sealed and attached together through apicolateral JC including tight junctions, adherens junctions, desmosome, and gap junctions along the lateral borders. (16) Exocytosis of heterophagic and autophagic byproducts into the BES evident at 17 Y. (**B**) The schema represents the contribution of heterophagy, autophagy and mitophagy in ensuring a viable and functional RPE-photoreceptor outer segment complex as evidenced by extensive ultrastructural observations throughout human fetal and early adolescent development. As the RPE develops it forms apical and basal infoldings. The apical microvilli accommodate rod and cone OS whereas the basal infoldings optimize cell surface area for exchange of metabolites with the choroidal circulation. Tight junctions, gap junctions, and desmosomes are formed to increase physical strength between the cells. Because of the dynamics of this structure, we see formation of the BES (*blue*). The photoreceptors are renewed daily by shedding their OS that are phagocytosed (heterophagosome) and digested through a process known as heterophagy. When single-membrane phagosomes fuse with single-membrane lysosomes, they form double-membrane heterophagosomes followed by single-membrane heterolysosomes where the process of digestion occurs. This process results in both digested materials able to be recycled by the RPE and undigested materials eventually forming single-membrane lipofuscin and deposition into the BES and drusen

located below the RPE and in the inner collagenous layer thereafter. Double-membrane autophagosomes/mitophagosomes are also formed by fusion of misfolded proteins and damaged organelles including dysfunctional mitochondria with lysosomes where the digestive process occurs through a process known as autophagy/mitophagy by formation of single-membrane autolysosomes/mitolysosomes. This also results in both recyclable materials and undigested components forming lipofuscin and eventually drusen. These metabolic demands on the RPE, in the basal region of the cell, encourage mitochondria to locate to this proximity. The recycling process occurs within the cytosol of the RPE cells. This schema represents the temporal region adjacent to the ONH in adolescence.

cell death by the apoptotic process of excess cells,[32] the earliest evidence of RPE apoptosis was observed at 10 WG. We showed that RPE cell diameter doubled between 12 and 16 WG. New cells are added by mitosis during early embryonic life[43]; however, RPE cells enlarge to fill in gaps created by apoptosis.

RPE cells produce type IV collagen, heparin sulphate, and laminin on their basal surfaces, which are incorporated into BrM formation.[44,45] The BrM has two major functions: acting as the substratum of the RPE while also functioning as the outer blood retinal barrier.[41] Although previous studies mentioned that four out of five layers of BrM can be distinguished as being continuous at 11 WG and only the elastic layer is not fully developed until 15 WG,[41,46,47] our findings show the primordial inner and outer collagenous and elastic layers are observed earlier (12 WG), followed by RPE and endothelial cell basal lamina development evident from 20 WG. This suggests that development of BrM follows a bidirectional pattern of formation where both the RPE and the choriocapillaris lay down basal lamina, which then forms BrM as the eye matures.

The human RPE serves numerous functions, including prevention of photo-oxidative toxicity through phagocytosis and digestion of POS.[9] Light first enters the eye at 26 WG, initiating POS phagocytosis with the first appearance of phagosomes. At 26 WG, because of an increase in light exposure with eye opening, the RPE protective mechanisms come into play. Melanosomes have a photoprotective role in the eye.[44,48,49] We showed that melanosomes migrate to the apical regions of the RPE to absorb light as it enters the RPE cells mitigating the deleterious effects of light scatter. Melanosomes are also capable of protecting RPE from damage caused by oxidative stress and light toxicity as they facilitate autophagy.[50] We observed that more than 60% migrate to the apical region, as well as accumulation of additional mitochondria in the inner segment of photoreceptors from 24 WG. This potentially provides evidence of an increase in ATP energy dependence on phototransduction.[51] This increase in phototransduction would create a further need for POS disc shedding, evidenced in this study by the presence of phagocytosis from 26 WG.

We provide evidence of phagosomes and complex granules at 26 WG, indicative of the initiation of phagocytosis. A remarkable finding of this study is that the initiation of phagocytosis of POS coincides with the initial period of eye opening at 26 WG, when the visually evoked potential, indicative of a functional visual pathway and photoreceptor activity, is also first detectable.[52] These critical findings and greater number of phagosomes near the ONH compared with mid periphery suggest that development of RPE functions initiate from the ONH. Phagocytosis is energy dependent[53–55] and increases the metabolic demands of RPE cells, creating a hypoxic environment and driving the increase in overall mitochondrial area centrally when compared to the periphery. The higher frequency of fenestrae and thinner basal lamina in the ONH compared to the periphery facilitates exchange of nutrients and elimination of byproducts, as supported by previous investigations.[56] This agrees with previous animal studies that showed RPE develops from the ONH to the periphery.[35,57,58]

Taken together, these findings lead us to conclude that the development of the human eye is functionally synchronized, enabling the initiation of retinal circuitry sustained by all supportive cellular elements, including the retinal[25] and choroidal vasculature,[25] glia,[26] and the RPE.

Because cytoplasmic remodeling through cell division does not occur in postmitotic cells,[59] the RPE depend on autophagy to eliminate protein aggregates, end of life organelles including mitochondrial alterations. This supports our hypothesis that increased RPE functions occurring after eye opening are associated with activation of autophagy from 32 WG.

The redistribution of mitochondria observed in this study is consistent with a recent study (Tabak 2023) that highlighted the ability of glioblastoma cancers to "steal" mitochondria from neighboring cells using active transport mechanisms involving actin filaments and energy (ATP). This is counter to the long-held belief that mitochondria generally "stayed put." Although our study only demonstrated the relocation of mitochondria within the same cell and not mitochondrial theft from a neighboring cell, it is still consistent with the concept that throughout RPE development, mitochondria have been observed to concentrate in different regions of the cell. Mitochondrial relocation potentially explains a greater need for energy consumption required to exocytose lipofuscin and other byproducts. The BES between adjacent RPE cells, which is identified from 26 WG, demonstrates a site for lipofuscin and byproduct deposition. It is generally accepted that the actin contraction path to move mitochondria is reliant on growth-associated protein 43, and this same mechanism may also be the pathway of subcellular organization underlying the mitochondrial relocalization to cytoplasmic regions of the RPE,[7,60] in an effort to meet the escalating energy demands of the complex heterophagic, autophagic, and mitophagic processes observed in differentiating cells.[61,62]

Our study provided compelling evidence that heterophagy and autophagy are both evident during the second trimester of human fetal development, where lipofuscin and autophagic byproducts form and are deposited in the BES. This study provided the first ultrastructural evidence of lipofuscin and autophagic byproduct formation and deposition in the BES as early as six years. Findings from our study demonstrate that the area of autophagosomes and autolysosomes increased with age during human fetal development through to adolescence, supportive of the conclusion that autophagy and heterophagy constitute core functions subserved by human RPE cells and that the ability of transplanted RPE to subserve these functions are essential for restoration of vision. It can become dysfunctional in the RPE when autophagosomes fuse with impaired lysosomes, adding to the accumulation of intracellular lipofuscin[61]

leading to RPE dysfunction and increased risk of AMD[63–65] as lipofuscin and byproducts are deposited in the BES.

Conclusions

This study undertook a semiquantitative ultrastructural characterization of development of the human RPE together with POS, BrM, and ChC maturation from eight WG to early adolescence. We showed that the processes required to sustain good vision throughout life are initiated with eye opening and the first exposure of the RPE to light stimulation. They include distinct migration of melanosomes apically and mitochondrial migration basally. Both heterophagy and autophagy are initiated to deal with byproducts of normal RPE functions. We observed BES formation and basal infolding of RPE cell membrane increasing the exchange area to facilitate absorption of nutrients and excretion of byproducts. We also observed the deposition of undigestible byproducts in the form of lipofuscin as young as six years of age. These developmental cellular processes are shown schematically in Figures 10A and 10B.

Numerous animal and human trials of RPE transplantation have been undertaken with the aim of restoring RPE and retinal functions but have met with limited functional success.[19–24,66,67] Allogenic or autologous ihRPE have been shown to demonstrate polarized specification and form apicolateral tight junctions and are capable of phagocytosis.[23] However, they failed to demonstrate the complex processes required to subserve heterophagy, autophagy, and exocytosis of byproducts. Because these additional functions are essential in restoring vision, our study provides a possible rationale for failure of these transplanted cells in restoring long-term vision.[19–21,23,66,67]

In summary, we suggest that for transplanted ihRPE cells to mitigate disease, they need to display the specific junctional complexes between adjacent RPE cells; display marked differentiation of organelles; demonstrate the polarity of normal human RPE cells, and, most importantly, have the capacity to subserve heterophagy and autophagy. The foundational importance of the transplanted ihRPE cells to be capable of autophagy is supported by the study showing that dysregulation of autophagy results in abnormal primary cilia, being the underlying pathogenetic mechanism for Leber's congenital amaurosis, an inherited retinal ciliopathy disease that often results in severe visual impairment or blindness in early childhood.[18] Transplantation of any type of RPE cells lacking these key functional properties, as demonstrated here for human fetal RPE development, could be responsible for failure to effectively restore vision. The *Nature Medicine* editorial "Of Men, Not Mice"[68] highlights how poorly mice reflect human disease and the importance to undertake normative studies using human tissues when gaining insights that form the basis for translation for future human therapies.

Acknowledgments

The authors thank Cedric Shorey and Robin Arnold from Discipline of Anatomy and The Bosch Institute at The University of Sydney for their expert advice and Sabine Grüninger from Department of Anatomical Pathology at ACT Pathology for her technical assistance.

Supported by grants to TCL from the National Health and Medical Research Council of Australia (Nos. 1005730 and 571100), the Baxter Charitable Foundation, Dr David Tai, the Alma Hazel Eddy Trust and the Rebecca L. Cooper Medical Research Foundation. SSD was the recipient of the NGW Macintosh Memorial Post-graduate research award and grant (2018) (Sydney, Australia).

Disclosure: **S. Shahhossein-Dastjerdi**, None; **M.E. Koina**, None; **G. Fatseas**, None; **F. Arfuso** None; **T. Chan-Ling**, None

References

1. Wong WL, Su X, Li X, et al. Global prevalence of age-related macular degeneration and disease burden projection for 2020 and 2040: a systematic review and meta-analysis. *Lancet Global Health*. 2014;2:e106–e116.
2. Beatty S, Koh H-H, Phil M, Henson D, Boulton M. The role of oxidative stress in the pathogenesis of age-related macular degeneration. *Surv Ophthalmol*. 2000;45:115–134.
3. Hall MO, Bok D, Bacharach A. Biosynthesis and assembly of the rod outer segment membrane system. Formation and fate of visual pigment in the frog retina. *J Mol Biol*. 1969;45:397–406.
4. Bok D, Hall MO. The role of the pigment epithelium in the etiology of inherited retinal dystrophy in the rat. *J Cell Biol*. 1971;49:664–682.
5. Bok D. The retinal pigment epithelium: a versatile partner in vision. *J Cell Sci*. 1993;1993:189–195.
6. Gao H, Hollyfield J. Aging of the human retina. Differential loss of neurons and retinal pigment epithelial cells. *Invest Ophthalmol Vis Sci*. 1992;33:1–17.
7. He Y, Ge J, Burke J, Myers R, Dong Z, Tombran-Tink J. Mitochondria impairment correlates with increased sensitivity of aging RPE cells to oxidative stress. *J Ocul Biol Dis Inform*. 2010;3:92–108.
8. Kaarniranta K, Sinha D, Blasiak J, et al. Autophagy and heterophagy dysregulation leads to retinal pigment epithelium dysfunction and development of age-related macular degeneration. *Autophagy*. 2013;9:973–984.
9. Kevany BM, Palczewski K. Phagocytosis of retinal rod and cone photoreceptors. *Physiology*. 2010;25:8–15.
10. Tombran-Tink J, Barnstable CJ. *Ocular transporters in ophthalmic diseases and drug delivery*. Berlin: Springer Science & Business Media; 2008.
11. Strauss O. The retinal pigment epithelium. *Physiol Rev*. 2005;85:845–881.
12. Bharti K, Miller SS, Arnheiter H. The new paradigm: retinal pigment epithelium cells generated from embryonic or induced pluripotent stem cells. *Pigment Cell Melanoma Res*. 2011;24:21–34.
13. Sparrow JR, Gregory-Roberts E, Yamamoto K, et al. The bisretinoids of retinal pigment epithelium. *Prog Retin Eye Res*. 2012;31:121–135.
14. Baba T, McLeod DS, Edwards MM, et al. VEGF 165b in the developing vasculatures of the fetal human eye. *Dev Dyn*. 2012;241:595–607.
15. Mazzoni F, Safa H, Finnemann SC. Understanding photoreceptor outer segment phagocytosis: use and utility of RPE cells in culture. *Exp Eye Res*. 2014;126:51–60.
16. Yorimitsu T, Klionsky DJ. Autophagy: molecular machinery for self-eating. *Cell Death Differ*. 2005;12(Suppl 2):1542–1552.
17. Luzio JP, Pryor PR, Bright NA. Lysosomes: fusion and function. *Nat Rev Mol Cell Biol*. 2007;8:622–632.
18. Chen HY, Swaroop M, Papal S, et al. Reserpine maintains photoreceptor survival in retinal ciliopathy by resolving proteostasis imbalance and ciliogenesis defects. *Elife*. 2023;12:e83205.

19. da Cruz L, Chen FK, Ahmado A, Greenwood J, Coffey P. RPE transplantation and its role in retinal disease. *Prog Retin Eye Res*. 2007;26:598–635.
20. Carr AJ, Vugler AA, Hikita ST, et al. Protective effects of human iPS-derived retinal pigment epithelium cell transplantation in the retinal dystrophic rat. *PLoS One*. 2009;4:e8152.
21. Ramsden CM, Powner MB, Carr A-JF, Smart MJ, da Cruz L, Coffey PJ. Stem cells in retinal regeneration: past, present and future. *Development*. 2013;140:2576–2585.
22. Mandai M, Watanabe A, Kurimoto Y, et al. Autologous induced stem-cell–derived retinal cells for macular degeneration. *N Engl J Med*. 2017;376:1038–1046.
23. da Cruz L, Fynes K, Georgiadis O, et al. Phase 1 clinical study of an embryonic stem cell-derived retinal pigment epithelium patch in age-related macular degeneration. *Nat Biotechnol*. 2018;36:328–337.
24. Sugita S, Mandai M, Kamao H, Takahashi M. Immunological aspects of RPE cell transplantation. *Prog Retin Eye Res*. 2021;84:100950.
25. Hughes S, Yang H, Chan-Ling T. Vascularization of the human fetal retina: roles of vasculogenesis and angiogenesis. *Invest Ophthalmol Vis Sci*. 2000;41:1217–1228.
26. Chu Y, Hughes S, Chan-Ling T. Differentiation and migration of astrocyte precursor cells (APCs) and astrocytes in human fetal retina: relevance to optic nerve coloboma. *FASEB J*. 2001;15:2013–2015.
27. Chan-Ling T, McLeod DS, Hughes S, et al. Astrocyte–endothelial cell relationships during human retinal vascular development. *Invest Ophthalmol Vis Sci*. 2004;45:2020–2032.
28. Chan-Ling T, Dahlstrom JE, Koina ME, et al. Evidence of hematopoietic differentiation, vasculogenesis and angiogenesis in the formation of human choroidal blood vessels. *Exp Eye Res*. 2011;92:361–376.
29. Chan-Ling T, Koina ME, McColm JR, et al. Role of CD44+ stem cells in mural cell formation in the human choroid: evidence of vascular instability due to limited pericyte ensheathment. *Invest Ophthalmol Vis Sci*. 2011;52:399–410.
30. Koina ME, Baxter L, Adamson SJ, et al. Evidence for lymphatics in the developing and adult human choroid. *Invest Ophthalmol Vis Sci*. 2015;56:1310–1327.
31. Streeten BW. Development of the human retinal pigment epithelium and the posterior segment. *Arch Ophthalmol*. 1969;81:383–394.
32. Rosenblatt J, Raff MC, Cramer LP. An epithelial cell destined for apoptosis signals its neighbors to extrude it by an actin-and myosin-dependent mechanism. *Curr Biol*. 2001;11:1847–1857.
33. Tawfik HA, Abdulhafez MH, Fouad YA, Dutton JJ. Embryologic and fetal development of the human eyelid. *Ophthalmic Plast Reconstr Surg*. 2016;32:407.
34. Bron AJ, Tripathi R, Tripathi B. *Wolff's Anatomy of the Eye and Orbit*. Abingdon, UK: Taylor & Francis. 1997.
35. Schoenwolf GC, Bleyl SB, Brauer PR, Francis-West PH. *Larsen's Human embryology*. 5th ed. New York: Churchill Livingstone; 2015.
36. Pollreisz A, Neschi M, Sloan KR, et al. Atlas of human retinal pigment epithelium organelles significant for clinical imaging. *Invest Ophthalmol Vis Sci*. 2020;61:13–13.
37. Pollreisz A, Messinger JD, Sloan KR, et al. Visualizing melanosomes, lipofuscin, and melanolipofuscin in human retinal pigment epithelium using serial block face scanning electron microscopy. *Experimental eye research*. 2018;166:131–139.
38. Ferrington DA, Sinha D, Kaarniranta K. Defects in retinal pigment epithelial cell proteolysis and the pathology associated with age-related macular degeneration. *Prog Retin Eye Res*. 2016;51:69–89.
39. Boya P. Why autophagy is good for retinal ganglion cells? *Eye (Lond)*. 2017;31:185–190.
40. Feeney L. Lipofuscin and melanin of human retinal pigment epithelium. Fluorescence, enzyme cytochemical, and ultrastructural studies. *Invest Ophthalmol Vis Sci*. 1978;17:583–600.
41. Curcio CA, Johnson M. Structure, function, and pathology of Bruch's membrane. In: Ryan SJ, Schachat AP, Wilkinson CP, Hinton DR, Sadda S, Wiedemann P, eds. *Retina*. 5th ed. London: Elsevier; 2013:466–481.
42. Efimova N, Svitkina TM. Branched actin networks push against each other at adherens junctions to maintain cell–cell adhesion. *J Cell Biol*. 2018;217:1827–1845.
43. Stroeva OG, Mitashov VI. Retinal pigment epithelium: proliferation and differentiation during development and regeneration. *Int Rev Cytol*. 1983;83:221–293.
44. Marmor MF, Wolfensberger TJ. *The Retinal Pigment Epithelium: Function and Disease*. New York: Oxford University Press, Inc.; 1998:776.
45. Kaufman PL, Levin LA, Adler FH, Alm A. *Adler's Physiology of the Eye*. Philadelphia: Elsevier Health Sciences; 2011.
46. Sellheyer K. Development of the choroid and related structures. *Eye*. 1990;4:255–261.
47. Johnson M, Curcio CA. Structure, function and pathology of Bruch's membrane. *Retina*. 6th ed. Elsevier; 2017:522–543.
48. Sarna T, Burke JM, Korytowski W, et al. Loss of melanin from human RPE with aging: possible role of melanin photooxidation. *Exp Eye Res*. 2003;76:89–98.
49. Wang Z, Dillon J, Gaillard E. Antioxidant properties of melanin in retinal pigment epithelial cells. *Photochemistry and photobiology*. 2006;82:474–479.
50. Schraermeyer U, Peters S, Thumann G, Kociok N, Heimann K. Melanin granules of retinal pigment epithelium are connected with the lysosomal degradation pathway. *Exp Eye Res*. 1999;68:237–245.
51. Wong-Riley M. Energy metabolism of the visual system. *Eye Brain*. 2010;2:99.
52. Dreher B, Robinson S. Development of the retinofugal pathway in birds and mammals: evidence for a common "timetable.". *Brain Behav Evol*. 1988;31:369–390.
53. Varner HH, Rayborn ME, Osterfeld AM, Hollyfield JG. Localization of proteoglycan within the extracellular matrix sheath of cone photoreceptors. *Exp Eye Res*. 1987;44:633–642.
54. Tien L, Rayborn ME, Hollyfield JG. Characterization of the interphotoreceptor matrix surrounding rod photoreceptors in the human retina. *Exp Eye Res*. 1992;55:297–306.
55. Iwasaki M, Myers KM, Rayborn ME, Hollyfield JG. Interphotoreceptor matrix in the human retina: cone-like domains surround a small population of rod photoreceptors. *J Comp Neurol*. 1992;319:277–284.
56. Lutty GA, Hasegawa T, Baba T, Grebe R, Bhutto I, McLeod DS. Development of the human choriocapillaris. *Eye*. 2010;24:408.
57. Provis JM, Van Driel D, Billson FA, Russell P. Development of the human retina: patterns of cell distribution and redistribution in the ganglion cell layer. *J Comp Neurol*. 1985;233:429–451.
58. Tsai J, Denniston A, Murray P, Huang J, Aldad T. *Oxford American Handbook of Ophthalmology*. Oxford, UK: Oxford University Press; 2011.
59. Rami A. autophagy in neurodegeneration: firefighter and/or incendiarist? *Neuropathol Appl Neurobiol*. 2009;35:449–461.
60. Ashrafi G, Schlehe JS, LaVoie MJ, Schwarz TL. Mitophagy of damaged mitochondria occurs locally in distal neuronal axons and requires PINK1 and Parkin. *J Cell Biol*. 2014;206:655–670.

61. Mitter SK, Rao HV, Qi X, et al. Autophagy in the retina: a potential role in age-related macular degeneration. *Retinal Degenerative Diseases*. Berlin: Springer; 2012:83–90.
62. Watson DC, Bayik D, Storevik S, et al. GAP43-dependent mitochondria transfer from astrocytes enhances glioblastoma tumorigenicity. *Nat Cancer*. 2023;1–17.
63. Pauleikhoff D, Barondes M, Minassian D, Chisholm I, Bird A. Drusen as risk factors in age-related macular disease. *Am J Ophthalmol*. 1990;109:38–43.
64. Holz FG, Schutt F, Kopitz J, et al. Inhibition of lysosomal degradative functions in RPE cells by a retinoid component of lipofuscin. *Invest Ophthalmol Vis Sci*. 1999;40:737–743.
65. Holz FG, Bindewald-Wittich A, Fleckenstein M, Dreyhaupt J, Scholl HPN, Schmitz-Valckenberg S. Progression of geographic atrophy and impact of fundus autofluorescence patterns in age-related macular degeneration. *Am J Ophthalmol*. 2007;143:463–472.e462.
66. Carr A-JF, Smart MJ, Ramsden CM, Powner MB, da Cruz L, Coffey PJ. Development of human embryonic stem cell therapies for age-related macular degeneration. *Trends Neurosci*. 2013;36:385–395.
67. Fuhrmann S, Zou C, Levine EM. Retinal pigment epithelium development, plasticity, and tissue homeostasis. *Exp Eye Res*. 2014;123:141–150.
68. Of men, not mice (editorial). *Nat Med*. 2013;19:379, https://doi.org/10.1038/nm.3163.